Accepted Manuscript

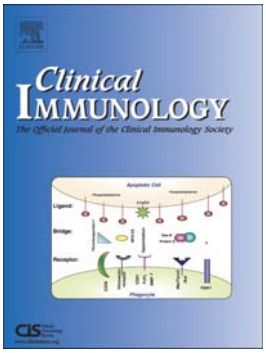

A non-invasive approach to monitor chronic lymphocytic leukemia engraftment in a xenograft mouse model using ultra-small superparamagnetic iron oxide-magnetic resonance imaging (USPIO-MRI)

Francesca Valdora, Giovanna Cutrona, Serena Matis, Fortunato Morabito, Carlotta Massucco, Laura Emionite, Simona Boccardo, Luca Basso, Anna Grazia Recchia, Sandra Salvi, Francesca Rosa, Massimo Gentile, Marco Ravina, Daniele Pace, Angela Castronovo, Michele Cilli, Mauro Truini, Massimo Calabrese, Antonino Neri, Carlo Emanuele Neumaier, Franco Fais, Gabriella Baio, Manlio Ferrarini

PII: S1521-6616(16)30176-0
DOI: doi: 10.1016/j.clim.2016.07.013
Reference: YCLIM 7693

To appear in: *Clinical Immunology*

Received date: 8 July 2016
Accepted date: 10 July 2016

Please cite this article as: Francesca Valdora, Giovanna Cutrona, Serena Matis, Fortunato Morabito, Carlotta Massucco, Laura Emionite, Simona Boccardo, Luca Basso, Anna Grazia Recchia, Sandra Salvi, Francesca Rosa, Massimo Gentile, Marco Ravina, Daniele Pace, Angela Castronovo, Michele Cilli, Mauro Truini, Massimo Calabrese, Antonino Neri, Carlo Emanuele Neumaier, Franco Fais, Gabriella Baio, Manlio Ferrarini, A non-invasive approach to monitor chronic lymphocytic leukemia engraftment in a xenograft mouse model using ultra-small superparamagnetic iron oxide-magnetic resonance imaging (USPIO-MRI), *Clinical Immunology* (2016), doi: 10.1016/j.clim.2016.07.013

A non-invasive approach to monitor chronic lymphocytic leukemia engraftment in a xenograft mouse model using ultra-small superparamagnetic iron oxide-magnetic resonance imaging (USPIO-MRI)

Authors:

Francesca Valdora[a,1,2], Giovanna Cutrona[a,1], Serena Matis[a], Fortunato Morabito[b,c], Carlotta Massucco[a], Laura Emionite[d], Simona Boccardo[e], Luca Basso[f], Anna Grazia Recchia[b,c], Sandra Salvi[e], Francesca Rosa[f], Massimo Gentile[b,c], Marco Ravina[g], Daniele Pace[g], Angela Castronovo[g], Michele Cilli[d], Mauro Truini[e,3], Massimo Calabrese[g], Antonino Neri[h,i], Carlo Emanuele Neumaier[g], Franco Fais[a,l,1], Gabriella Baio[g,1,4] , Manlio Ferrarini[m,1*]

Author information

[a] Molecular Pathology, IRCCS- A.O.U. San Martino – IST, Largo Rosanna Benzi 10, 16132 Genoa, Italy (Valdora F.; Cutrona G.; Matis S.; Massucco C.; Fais F. E-mail: valdorafrancesca@gmail.com; giovanna.cutrona@gmail.com; serena.matis@hsanmartino.it; carlotta.massucco@libero.it; franco.fais@unige.it)

[b] Hematology Unit, Department of Onco-Hematology, A.O. of Cosenza, Cosenza, Italy (Morabito F.; Recchia A.G.; Gentile M. E-mail: fortunato_morabito@tiscali.it; annarecchia@tin.it; massim.gentile@tiscali.it)

[c] Biotechnology Research Unit, Aprigliano, A.O./ASP of Cosenza, Cosenza, Italy;

[d] Animal Facility, IRCCS -A.O.U. San Martino – IST, Largo Rosanna Benzi 10, 16132 Genoa, Italy (Emionite L.; Cilli M. E-mail: laura.emionite@hsanmartino.it; michele.cilli@hsanmartino.it)

[e] Division of Histopathology and Cytopathology, IRCCS-A.O.U. San Martino– IST, Largo Rosanna Benzi 10, 16132 Genoa, Italy (Boccardo S.; Salvi S.; Truini M. E-mail: simona.boccardo@hsanmartino.it; sandra.salvi@hsanmartino.it; mauro.truini@ospedaleniguarda.it)

[f] Department of Science of Health (DISSAL), University of Genoa, Via Antonio Pastore 1, 16132 Genoa, Italy (Basso L.; Rosa F. E-mails: lukabasso89@gmail.com; francescarosa892@gmail.com)

[g] Diagnostic Imaging and Senology, IRCCS-A.O.U. San Martino–IST, Largo Rosanna Benzi 10, 16132 Genoa, Italy (Calabrese M.; Neumaier CE.; Baio G.; Ravina M.; Pace D.; Castronovo A. E-mail: massimo.calabrese@hsanmartino.it; carlo.neumaier@gmail.com; gabriella.baio@abdn.ac.uk; marco.ravina@hsanmartino.it; daniele.pace@hsanmartino.it; angela.castronovo@hsanmartino.it)

[h] Department of Oncology and Hemato-Oncology, University of Milano, Milan, Italy (Neri A. E-mail: antonino.neri@unimi.it)

[i] Hematology Unit, Fondazione IRCCS Ca' Granda, Ospedale Maggiore Policlinico, Milan, Italy.

[l] Department of Experimental Medicine - University of Genoa, Genoa, Italy (Fais F.)

[m] Scientific Direction, IRCCS-A.O.U. San Martino – IST, Genoa, Italy (Ferrarini M. E-mail: manlio.ferrarini@hsanmartino.it)

*__Corresponding author__: Manlio Ferrarini, MD, Scientific Director, IRCCS A.O.U. San Martino – IST, Largo Rosanna Benzi 10, 16132 Genoa, Italy;

E-mail address: manlio.ferrarini@hsanmartino.it

1

[1] These authors have contributed equally to the work.
[2] Present address: Department of Experimental Medicine - University of Genoa, Genoa, Italy
[3]Present address: Department of Hematology & Oncology, Niguarda Cancer Center, Ospedale Niguarda Ca' Granda, Milan, Italy
[4]Present address: Aberdeen Biomedical Imaging Centre, University of Aberdeen, Aberdeen, UK

Abstract:

Chronic lymphocytic leukemia (CLL) is the most prevalent leukemia among adults. Despite its indolent nature, CLL remains an incurable disease. Herein we aimed to monitor CLL disease engraftment and,progression/regression in a xenograft CLL mouse model using ultra-small superparamagnetic iron oxide-magnetic resonance imaging (USPIO-MRI). Spleen contrast enhancement, quantified as percentage change in signal intensity upon USPIO administration, demonstrated a difference due to a reduced USPIO uptake, in the spleens of mice injected with CLL cells (NSG-CLL, n=71) compared to controls (NSG-CTR, n=17). These differences were statistically significant both after 2 and 4 weeks from CLL cells injection. In addition comparison of mice treated with rituximab with untreated controls for changes in spleen iron uptake confirmed that it is possible to monitor treatment efficacy in this mouse model of CLL using USPIO-enhanced MRI. Further applications could include the preclinical *in vivo* monitoring of new therapies and the clinical evaluation of CLL patients.

Keywords

Chronic Lymphocytic Leukemia (CLL); Magnetic Resonance Imaging (MRI); Ultra-small Superparamagnetic Iron Oxide (USPIO); Xenograft NSG mice model; Disease monitoring.

Abbreviations

MRI, Magnetic Resonance Imaging; ROI, Region of Interest; CLL, Chronic lymphocytic leukemia; USPIO, Ultra-small Superparamagnetic Iron Oxide; SNR, Signal-to-Noise ratio; CT, Computed Tomography; SD, Standard Deviation; sem, standard error of mean; SI, Signal Intensity; ΔSNR%, percentage Signal-to-Noise ratio change; i.v., intravenous injection; i.p., intraperitoneal injection; RES, Reticulo-Endothelial System; PBMC, peripheral blood mononuclear cells; FC, Flow Cytometry; MHz, MegaHerzt; FIESTA, Fast Imaging Employing Steady State Acquisition; FA, Flip Angle; FoV, Field of view; TR, repetition time; TE, echo time; T1, longitudinal relaxation time; T2, transverse relaxation time; ROC, receiver-operating characteristic; CI, confidence interval. IGHV, immunoglobulin heavy chain variable region; FISH, fluorescent in situ hybridization.

Units

Mm, millimetre; g, gram; Mg, milligram; Kg, kilogram; µL, microliter; µmol, micromole; ms, millisecond; nm, nanometer; min, minute; °C, Centigrade.

1. Introduction

Chronic lymphocytic leukemia (CLL) is the most common form of adult leukemia in Western countries [1, 2]. CLL is characterized by the clonal expansion of mature CD5+/CD23+ lymphocytes that can infiltrate multiple organs including lymph nodes, the bone marrow, spleen, and liver. CLL is highly heterogeneous in terms of therapy-free interval, response to treatment and overall survival, ranging from rapid disease progression requiring early and frequent treatment, to survival for decades with minimal or no treatment. Staging of CLL patients involves periodical evaluation of lymph nodes, spleen, and liver infiltration and is used to define risk and treatment. Follow-up generally includes a blood cell count and palpation of lymph nodes, liver, and spleen every 3-12 months [3, 4]. In daily clinical practice, a common modality for evaluating changes in spleen size is to assess if the spleen is palpable, which means that the spleen generally requires an enlargement of at least two folds in order for changes to be detected. In addition, unlike superficial lymph nodes, deep nodes cannot be evaluated by simple palpation alone.

Several mouse models for the study of CLL development have been established[5]. These encompass transgenic models in which key genes have been altered [6-9]or xenograft models that use immunodeficient mice that are engrafted with human leukemic cells [10-12]. In all instances, development of the CLL clone can be followed by monitoring peripheral blood for the presence of leukemic cells, but the evaluation of lymphoid tissues (i.e. the spleen, in immunodeficient mice as lymph-nodes are mostly atrophic), where the leukemic cells have to seed to begin their proliferative phase, requires sacrificing the animals. Thus, sensitive and safe imaging techniques to monitor disease development may be useful in preclinical models and, more importantly also based on the above considerations, may find application in routine clinical practice.

Computer tomography (CT) is used as the first-line modality for imaging of lymphoid malignancies [13]. The role of CT has not been clearly defined in CLL patients, although CT routine disease monitoring for CLL has been largely discouraged [3, 14, 15]. CT scans are recommended for baseline and final assessment in clinical trials and is not the method of choice to be used in clinical staging [16, 17]. Magnetic resonance imaging (MRI) has a high sensitivity in the diagnosis of the disease and also plays an important role in the assessment of disease activity without the need for exposure to ionizing radiation. The success of MRI *in vivo* highly depends on the molecular imaging agent used. With the help of efficient imaging agents, it is possible for MRI to precisely detect early-stage disease and to monitor the response to drug therapy.

Superparamagnetic iron oxide (SPIO) or ultra-small superparamagnetic iron oxide (USPIO) nanoparticles are now primarily used and are becoming increasingly attractive as the precursor for the development of a target-specific MRI contrast agent in molecular MRI. The efficacy of iron

oxide nanoparticles used as specific contrast agent in MRI for liver, spleen, and lymph node has been demonstrated in experimental and clinical studies. Several studies have shown that these particles can significantly improve the detection and characterization of focal lesions within these organs [18-20]. Due to their size-dependent properties and their applicability in non-invasive imaging methods, these materials are promising candidates for research, diagnostic, and therapeutic applications in various fields such as cancer, neurodegenerative diseases (e.g. multiple sclerosis, [21-23], stroke [24, 25]), as well as in inflammatory diseases (e.g. rheumatoid arthritis [26] and atherosclerosis [27]). Iron oxide particles can be used as contrast medium in MRI because they are agents of high relaxivity able to enhance the contrast in T2/T2*-weighted MRI in tissues in which they accumulate. USPIO are taken up by the cells of the liver, spleen, bone marrow, and lymph nodes. Because of their small size (mean size 10-20 nm), they diffuse freely through capillaries and are phagocytized by tissue-resident inflammatory cells of the reticulo-endothelial system (RES), which predominantly consists of macrophages, although neutrophils may also take up USPIO [28-30].

In this study we aimed to establish a non-invasive specific MRI method to better visualize and to quantify the presence of CLL disease by USPIO within the spleen in a pre-clinical setting. In particular, we used a mouse xenogeneic transplantation model, NOD/Shi-scid, γc^{null} (NSG) mice, a NOD/SCID-derived strain that lacks the IL-2 family common cytokine receptor gamma chain gene (γc) [10, 11]. A secondary goal was to monitor CLL disease evolution using imaging strategies in an attempt to reduce the overall number of mice necessary for the evaluation of CLL cell engraftment over several time points, limiting their sacrifice and suffering during experimental protocols.

2. Materials and Methods

2.1 CLL Patients

Newly diagnosed CLL patients from participating Institutions were enrolled within 12 months from diagnosis (O-CLL1 protocol clinicaltrial.gov identifier NCT00917540). Diagnosis was confirmed by flow cytometry (FC) analysis centralized at the National Institute of Cancer Laboratory in Genoa, Italy, together with the determination of CD38 and ZAP-70 expression and IGHV mutational status as previously described [31, 32]. Cytogenetic abnormalities involving deletions at chromosomes (11)(q22.3), (13)(q14.3) and (17)(p13.1), and trisomy 12 were evaluated by fluorescent in situ hybridization (FISH) in purified CD19+ population as previously described[32] (Table 1).

PBMC from patients with CLL were isolated by Ficoll-Hypaque (Seromed, Biochrom) density gradient centrifugation.

2.2 Murine model

Six to eight week old female NOD/Shi-scid,γc^{null} (NSG) mice (The Jackson Laboratory), a xenograft model for CLL growth *in vivo* [10, 11], were housed in sterile enclosures under specific pathogen-free conditions. All procedures involving animals were performed respecting the current National and International regulations and were reviewed and approved by the licensing and Animal Welfare Body of the IRCCS-AOU San Martino-IST National Cancer Research Institute, Genoa, Italy.

NSG mice were infused by intravenous injection (i.v.) with 30-50x10^6 PMNCs/mouse from 18 CLL cases (see Table 1) and the presence of CD19+CD5+ leukemic cells were checked after 2 and 4-weeks from the date of injection in blood samples taken from the retro-orbital vein.

2.3 Preparation of USPIO particles-contrast agent and dosage

The USPIO contrast agent (Feraspin XS, Miltenyi Biotech GmbH, Germany) used, consists of commercially available USPIO nanoparticles with a mean particle size of 10-20 nm, able to circulate in the bloodstream and be taken up by RES macrophages.. All animal groups were imaged before, and 24 hours after i.v injection of 100 µL/25 g mouse of USPIO, corresponding to a dose of 40 µmol Fe/kg body weight.

2.4 In-vivo MRI experiments

The mice were anesthetized by intraperitoneal injection (i.p.) with a combination of xylazine (30mg/kg) and ketamine (100mg/kg) and were positioned in a prototype coil (birdcage linear coil, transmit/receive coil, 100 mm in length, 55 mm in diameter, tuned at 127.6 MHz, Flick Engineering Solutions BV, Milwaukee, USA). The room temperature during experiments was 23°C and the mean acquisition time was limited to 20 min by the spontaneous awakening of mice. *In vivo* MRI was performed on a 3T clinical system (Sigma® EXCITE® HDxT, GE Healthcare, Milwaukee, USA). The approved imaging protocol is described in Table S1. The saline solution was administrated before and after MRI scanning in order to rehydrate the mice and to alleviate pain. After completion of the MRI, all mice were sacrificed in a saturated CO2 chamber and autopsies were performed. The spleens were collected for IHC analysis and cytofluorimetric analysis.

2.5 MRI Signal Intensity Analysis

All animal groups were imaged before and 24 hours after USPIO administration as described above. Both qualitative and quantitative analyses were performed with FIESTA (Fast Imaging Employing Steady State Acquisition)-weighted sequences [33]. Quantitative analyses were expressed as Signal Intensity (SI) ± standard deviation (SD) for each mouse, calculated 24 hours after Feraspin XS administration, with SI being measured in the spleen, and the background noise was determined by drawning a region outside the anatomy of the mice, using an operator-defined region of interest (ROI). Circular ROIs were manually drawn and the size of the ROIs were measured by consistently acquiring the same size in the control group and in mice injected with CLL cells. After defining the ROIs, the SI in the spleen of each mouse was acquired. A circular ROI, positioned as indicated in Fig. 1, was used to calculate the signal-to-noise ratio (SNR) and ΔSNR% as follows [34, 35]:

$SNR = SI_{tissue}/SI_{noise}$

$\Delta SNR\% = [(SNR_{\text{after USPIO}}) - (SNR_{\text{before USPIO}})/ SNR_{\text{before USPIO}}]*100$

2.6 Histopathological analysis

Formalin-fixed and paraffin-embedded spleen specimens were analyzed for the presence of human CLL infiltrates. The sections were deparaffined and antigen-retrieval was performed with citrate buffer high pH for 8 minutes. Double staining with CD20 and Ki67 by IHC was performed by incubation (32 min at 37°C) with a specific anti-human Ki67 antibody (MIB-1, DAKO Cytomation, dilution 1:25) and followed by addition of the polymeric detection system Ultraview Universal DAB Detection Kit (Roche, Ventana).-Automatic dispensing of the second antibody (anti-CD20, L26- Roche Ventana Medical System) for 20 minutes at 37°C, was followed by addition of the polymeric detection system (Ultraview Universal RED Detection Kit). An appropriate positive tissue control was used for each staining run; the negative control consisted of performing the entire IHC procedure on adjacent sections in the absence of the primary antibody. The sections were counter-stained (automatically using a user-defined protocol) with Gill's modified hematoxylin and then cover-slipped. All sections were quantitatively evaluated by two observers with an Olympus light microscope using 10 X, 40 X and 63 X objectives. All the sections were analyzed under a Leica DM3000 DMLB optical microscope (Leica Microsystems, Germany) and microphotographs were collected using a Leica DFC320 DMD108 digital microimaging camera (Leica Microsystems, Germany). Perls' Prussian blue staining (Histological staining Kit, code 010236, Diapath) was performed to detect ferric (Fe3+) iron.

2.7 Treatment with rituximab

CLL engraftment was achieved as described above. The anti-CD20 MAb, Rituximab, was donated by the pharmacy of our Institution from remnants of the patients' sack therapy. Rituximab treatment was started using a dosage of 50 µg/mouse/dose (four treatments every 3 days) in 200µl of saline solution by i.v. injection [36]. The control group was injected with an equal volume of saline solution. Basal MRI was performed after four weeks of PBMC CLL injection before starting therapy and thereafter, at therapy completion [treated mice (n=3), control mice (n=3)] treated with saline solution as detailed in supplementary Fig. 1.

After three days of the last dose of antibody, animals were sacrificed in a saturated CO2 chamber and autopsies were performed. Blood, and different samples of the spleens were evaluated by both FC and by IHC as described above. Fresh spleen tissue samples were mechanically resuspended with gentleMACS™ Dissociator (Miltenyi). The spleens were previously enzymatically digested using the Spleen Dissociation Kit (Miltenyi). The single-cell suspensions were evaluated by flow cytometry analysis with FACSCanto (BD Biosciences) and DIVA 6 (BD Biosciences) or FLOWJO V.9.8.3 software (Treestar Inc.) for: anti-human (hu) CD45 FITC, CD19 PECy7, CD5 APC antibodies (BD Biosciences).

2.8 Statistical analysis

The U-Mann Whitney statistical test was used for testing statistical differences between more than two groups of samples and the Wilcoxon test for matched-pairs groups.

In order to identify the best cut-off value to be used in our experiments able to discriminate engrafted disease from engraftment failure, a diagnostic threshold of the relative enhancement measurements was sought by constructing receiver operating characteristic (ROC) curves. In an ROC curve, the true-positive rate (sensitivity) is plotted as a function of the false-positive rate (100 specificity) for different cut-off points. Each point on the ROC plot represents a sensitivity and specificity pair that corresponds to a particular decision threshold. The area under the ROC curve (AUROC) was analyzed to define the performance of the applied methods. The 95% confidence intervals (CI) were calculated (see supplementary Fig.2). A value of $P<0.05$ was considered significant for all statistical calculations. Values are given as means ± sem.

3. Results

3.1 MRI signal measurements and histopathological correlations

NSG mice were inoculated with CLL cells and autologous T cells (defined as NSG-CLL) to favor the engraftment of the leukemic clones. USPIO-enhanced MRI was performed after two weeks and/or after four weeks in control mice (NSG-CTR, mice that did not receive any human cells), and in the NSG-CLL mice; results were expressed as ΔSNR%.

Overall, twenty-four hours after USPIO administration we observed an increase in SI in the NSG-CLL at two weeks (n=41) and at four weeks (n=28) compared to the NSG-CTR mice. In Fig. 2 two representative experiments of mice analyzed at four weeks are shown. Fig. 2A and 2D show MRI images of NSG-CTR and NSG-CLL after 24 h of USPIO administration. Fig. 2B and 2E show spleen IHC analysis of the same mice displaying the absence of CD20+ cells in NSG-CTR mice and the presence of focal aggregates of CD20 positive cells in NSG-CLL spleen surrounded by CD3+ cells (not shown). In addition, Perls' Prussian blue staining (used to detect USPIO nanoparticles) indicated that ferric iron particles were excluded from the focal lesions (Fig 2F) whereas a random distribution of USPIO nanoparticles was observed in the spleens of NSG-CTR mice (Fig 2C).

Fig. 3 summarizes the data obtained from all NSG mice analyzed including those that did not achieve engraftment [defined as NSG non-engrafted mice, (NSG-CLL-ne)] as demonstrated by the absence of CD20+ and CD3+ cells when sacrificed for IHC and FC examination of the spleen at four weeks (data not shown). In addition, at this time, their peripheral blood did not show presence of huCD45+ cells (data not shown). The U-Mann Whitney statistical test found a significant difference ($P<0.0001$) comparing the group of NSG-CTR mice to NSG-CLL mice at four weeks. Interestingly, a significant difference was also observed when comparing the NSG-CLL mice at two weeks ($P<0.0001$) (Fig. 3A). Significant differences were also observed comparing measurements of the same NSG-CLL mice at two and four weeks from PBMC CLL injection (Fig. 3B).

3.2 Cut-off determination

ROC analysis was utilized in order to identify the best cut-off for ΔSNR% to be used in our experiments for discriminating NSG-CLL mice from NSG-CTR. The best cut-off values were -4.8 (AUC = 0.97 [95%CI 0.92-1.0]) at 2 weeks and -6.0 (AUC = 0.99 [95%CI 0.97-1.0]) at 4 weeks. (Supplementary Fig.2).

3.3 Measurements of CLL disease regression in NSG engrafted mice.

In order to investigate whether this technique would be useful for evaluating CLL disease regression upon therapy, NSG-CLL mice were treated with rituximab. Four mice were treated four

times at three-day intervals using a dosage of 50 µg/mouse, and compared with five mice injected with an identical volume of saline solution (mock-treated mice).

MRI was carried out in three mock-treated NSG-CLL mice and in three NSG-CLL treated with rituximab and the relative signal measurements obtained at therapy start were compared with those obtained at therapy completion (Fig. 4). The ΔSNR% values showed a clear reduction in animals treated with rituximab compared to mock-treated animals (Fig. 4C and 4D). Differences did not reach statistical significance likely due to the limited number of animals investigated. The general strategy of treatments and spleen evaluations is shown in Supplementary Fig.1.

Spleen IHC analysis for expression of CD20, Ki67, CD3, and Perls' Prussian blue staining of mice treated with rituximab or with saline solution are shown in Fig. 5A and 5B. Spleen tissue IHC indicates that the decreased MRI signal observed in rituximab-treated mice correlates with the loss of CD20+ cells organized in follicles (clearly observable in the spleen of mock-treated NSG-CLL mice). In addition, follicle residues are clearly infiltrated by T cells and USPIO nanoparticles (Fig. 5B). Spleen FC analysis showed that huCD45/CD19/CD5+ cells were significantly less represented in rituximab-treated mice compared to mock-treated mice. In contrast, the percentage of CD3-positive cells was significantly higher in mock-treated mice, compared to NSG-CLL mice treated with rituximab (Fig. 5C and 5D).

4. Discussion

MRI is a well-suited imaging modality for noninvasive cell tracking because of its tissue characterization, excellent image quality, and high spatial resolution, although currently nuclear imaging is a more sensitive technique. Furthermore, MRI advantages include lack of ionizing radiation, flexible image contrast, and the ability to assess localized function, perfusion, and necrosis. MRI offers the potential of tracking cells *in vivo* using innovative approaches and contrast media as well as cell labeling and image acquisition.

In this study, we used MRI to track CLL cell seeding in a xenograft mouse model. We first observed that changes in spleen organization could be identified four weeks after CLL cell inoculation and analyzed by means of a high field 3T clinical scanner and USPIO nanoparticles. We used FIESTA acquisition because our previous observations indicated that it was suitable and also high sensitive in conditions of very low iron oxide nanoparticle concentrations [37] rendering this sequence the best option for the study of single cell iron oxide nanoparticles [33]. Histologic examination of the same spleens confirmed the presence of CD20+ nodular structures (see Fig. 2) surrounded by CD3+ cells (not shown). In addition, Perls' Prussian blue staining demonstrated that iron particles were excluded from the nodular areas occupied by lymphoid cells, providing a

rational explanations for the MRI signals observed. The combination of extracellular with intracellular iron oxide nanoparticles compartmentalization within the CLL spleen, affected iron oxide proton relaxivity, which sometimes resulted in an increase rather than in the usual and expected SI decrease. This high T2-USPIO effect has also been reported by Simon G.H. et al [38]. FC analyses of splenic cell suspensions showed that huCD45+ cells were comprised of CD19/CD5+ cells and a variable proportion of CD3+ cells (not shown). An analogous approach of using FC to measure circulating T and B cells can be employed to assess the take of CLL engraftment in NSG mice although this method may be misleading, as leukemic cells can be difficult to track due to their extremely low number in peripheral blood. In addition, when tracked, the leukemic cells may represent cells merely surviving after the injection. Indeed, 17/19 non engrafted mice showed the presence of huCD45/CD19/CD5 cells (representing the bona fide the leukemic clone). In contrast USPIO enhanced MRI spleen analysis was able to consistently assess the engraftment of CLL cells two weeks after their injection (see Fig. 3), as could also be confirmed by IHC evaluation.

A reliable assessment of CLL engraftment two weeks after leukemic clone inoculation is most advantageous given that this animal model does not allow long term persistence/expansion of the inoculated leukemic cells beyond 6-8 weeks. Thereafter, mice can develop a graft-versus-host disease that may cause also the reduction and even disappearance of the leukemic cells [11]. In addition, leukemic cells can mature intointo plasmablasts/plasmacells [39]. The above limitations might impair the experimental data, particularly when drug treatments are evaluated, because this time-frame may not be sufficient to provide information on the long term effect of drugs.

We also report the possibility of identifying a cut-off value for ΔSNR% able of discriminating NSG-CLL from NSG-CTR or NSG-ne mice. A similar cut-off value was used to identify the different disease extension at two and four weeks after inoculum in NSG-CLL mice. The identification of a relatively precise cut-off value allows investigators to reliably define when a single mouse can be considered engrafted or not and make decisions regarding the subsequent experimental procedures. This analysis however requires standardization on the instrument(s) used for the image acquisition.

USPIO-enhanced MRI also was able to detect CLL disease regression after rituximab treatment of engrafted mice. MRI images, acquired before and following treatment, MRI images detected definite changes with an inversion of the ΔSNR% value (see Fig. 4). IHC showed a radical change in the architecture of the spleen of treated animals compared to controls. Following treatment, lymphoid infiltrates were mainly represented by unorganized T lymphocytes with the loss of the typical CD20+ nodular areas. Tissue Perls' Prussian blue stain confirmed the diverse disposition of

USPIO nanoparticles (Fig. 5). Thus, this technique clearly distinguishes between the different types of lymphoid infiltrates on the basis of their organization.

Another point that should be underlined is that the use of this technique limits the number of animals to be tested and sacrificed. This is important for several reasons: first, it requires fewer leukemic cells for injection thus sparing other cells for additional experimental procedures. Although a large number of CLL cells can generally be recovered from CLL patients, a typical experiment may require more than half a billion cells, a quantity often obtained from selected patients only. Second, this approach facilitates clearance of animal experimentation protocols by ethics committees. Currently, animal testing regulations pay increasingly more attention to the procedures and the experimental settings applied, encouraging the use of methods that limit animal sacrifice (and ultimately suffering of animals). A related point is the control of experimental variability, as only animals with evidence of disease are used to complete the experimental procedures with no additional trauma.

5. Conclusions

In summary, we present here an *in vivo* imaging approach for monitoring CLL disease evolution in a pre-clinical model of CLL using xenografted immunodeficient mice. MRI is a valuable, non-invasive modality to predict progression in our CLL-model. In addition, by anticipating the timing of CLL engraftment, applications of MRI may include *in vivo* monitoring of new therapies thus allowing a longer temporal window to evaluate treatment efficacy and the possible emergence of therapy resistant clones.

Finally, this method may have potential application in the clinical setting and may be used to evaluate organ involvement in CLL disease, allowing more accurate staging without exposing patients to additional radiation.

Conflicts of interest

The authors declared no conflict of interest.

Acknowledgements

In addition to the listed Authors, the following Investigators participated in this study as part of the GISL - Gruppo Italiano Studio Linfomi: Gianni Quintana, Divisione di Ematologia, Presidio Ospedaliero "A.Perrino", Brindisi; Giovanni Bertoldero, Dipartimento di Oncologia, Ospedale Civile, Noale, Venezia; Paolo Di Tonno, Dipartimento di Ematologia, Venere, Bari; Robin Foà and Francesca R Mauro, Divisione di Ematologia, Università La Sapienza, Roma; Nicola Di Renzo, Unità di Ematologia, Ospedale Vito Fazzi, Lecce; Maria Cristina Cox, Ematologia, A.O. Sant'Andrea, Università La Sapienza, Roma;Stefano Molica, Dipartimento di Oncologia ed Ematologia, Pugliese-Ciaccio Hospital, Catanzaro; Attilio Guarini, Unità di Ematologia e Trapianto di Cellule Staminali, Istituto di Oncologia "Giovanni Paolo II", Bari; Antonio Abbadessa, U.O.C. di Oncoematologia Ospedale "S. Anna e S. Sebastiano", Caserta; Francesco Iuliano, U.O.C. di Oncologia, Ospedale Giannettasio, Rossano Calabro, Cosenza; Omar Racchi, Ospedale Villa Scassi Sampierdarena, Genova; Mauro Spriano, Ematologia, A.O. San Martino, Genova; Felicetto Ferrara, Divisione di Ematologia, Ospedale Cardarelli, Napoli; Monica Crugnola, Ematologia, CTMO, Azienda Ospedaliera Universitaria di Parma; Alessandro Andriani, Dipartimento di Ematologia, Ospedale Nuovo Regina Margherita, Roma; Nicola Cascavilla, Unità di Ematologia e Trapianto di Cellule Staminali, IRCCS Ospedale Casa Sollievo della Sofferenza, San Giovanni Rotondo; Lucia Ciuffreda, Unità di Ematologia, Ospedale San Nicola Pellegrino, Trani; Graziella Pinotti, U.O. Oncologia Medica, Ospedale di Circolo Fondazione Macchi, Varese; Anna Pascarella, Unità Operativa di Ematologia, Ospedale dell'Angelo, Venezia-Mestre; Maria Grazia Lipari, Divisione di Ematologia, Ospedale Policlinico, Palermo, Francesco Merli, Unità Operativa di Ematologia, A.O.S. Maria Nuova, Reggio Emilia; Luca Baldini Istituto di Ricovero e Cura a Carattere Scientifico Cà Granda-Maggiore Policlinico, Milano; Caterina Musolino, Divisione di Ematologia, Università di Messina; Agostino Cortelezzi, Ematologia and CTMO, Foundation IRCCS Ca' Granda Ospedale Maggiore Policlinico, Milano; Francesco Angrilli, Dipartimento di Ematologia, Ospedale Santo Spirito, Pescara; Ugo Consoli, U.O.S. di Emato-Oncologia, Ospedale Garibaldi-Nesima, Catania; Gianluca Festini, Centro di Riferimento Ematologico-Seconda Medicina, Azienda Ospedaliero-Universitaria, Ospedali Riuniti, Trieste; Giuseppe Longo, Unità di Ematologia, Ospedale San Vincenzo, Taormina; Daniele Vallisa and Annalisa Arcari, Unità di Ematologia, Dipartimento di Onco-Ematologia, Guglielmo da Saliceto Hospital, Piacenza; Francesco Di Raimondo and Annalisa Chiarenza, Divisione di Ematologia, Università di Catania Ospedale Ferrarotto, Catania; Iolanda Vincelli, Unità di Ematologia, A.O. of Reggio Calabria; Donato Mannina, Divisione di Ematologia, Ospedale Papardo, Messina, Italy.

We would thank Gerolama Buconte for her very helpful technical support for the MRI acquisition and Dr Marcella Bado, Dr Barbara Rebesco for providing rituximab preparations.

Funding: This work was supported by: Associazione Italiana Ricerca sul Cancro (AIRC) [Grant 5 x mille n.9980, (to M.F., F.M. and A. N.)]; AIRC I.G. [n. 14326 (to M.F.)], [n.10136 and 16722 (A.N.)], [n.15426 (to F.F.)]. AIRC and Fondazione CaRiCal co-financed Multi Unit Regional Grant 2014 [n.16695 (to F.M.)]. Italian Ministry of Health 5x1000 funds (to F.F). A.G R. was supported by Associazione Italiana contro le Leucemie-Linfomi-Mielomi (AIL) Cosenza - Fondazione Amelia Scorza (FAS). S.M. C.M., F.V., L. E., S. B., were supported by AIRC.

References

[1] N. Chiorazzi, K.R. Rai, M. Ferrarini, Chronic lymphocytic leukemia, The New England journal of medicine, 352 (2005) 804-815.

[2] M.J. Keating, Chronic lymphocytic leukemia, Semin Oncol, 26 (1999) 107-114.

[3] M. Hallek, B.D. Cheson, D. Catovsky, F. Caligaris-Cappio, G. Dighiero, H. Dohner, P. Hillmen, M.J. Keating, E. Montserrat, K.R. Rai, T.J. Kipps, L. International Workshop on Chronic Lymphocytic, Guidelines for the diagnosis and treatment of chronic lymphocytic leukemia: a report from the International Workshop on Chronic Lymphocytic Leukemia updating the National Cancer Institute-Working Group 1996 guidelines, Blood, 111 (2008) 5446-5456.

[4] S. Kempin, Update on chronic lymphocytic leukemia: overview of new agents and comparative analysis, Curr Treat Options Oncol, 14 (2013) 144-155.

[5] S.E. Herman, A. Wiestner, Preclinical modeling of novel therapeutics in chronic lymphocytic leukemia: the tools of the trade, Semin Oncol, 43 (2016) 222-232.

[6] R. Bichi, S.A. Shinton, E.S. Martin, A. Koval, G.A. Calin, R. Cesari, G. Russo, R.R. Hardy, C.M. Croce, Human chronic lymphocytic leukemia modeled in mouse by targeted TCL1 expression, Proc Natl Acad Sci U S A, 99 (2002) 6955-6960.

[7] J.M. Zapata, M. Krajewska, H.C. Morse, 3rd, Y. Choi, J.C. Reed, TNF receptor-associated factor (TRAF) domain and Bcl-2 cooperate to induce small B cell lymphoma/chronic lymphocytic leukemia in transgenic mice, Proc Natl Acad Sci U S A, 101 (2004) 16600-16605.

[8] U. Klein, M. Lia, M. Crespo, R. Siegel, Q. Shen, T. Mo, A. Ambesi-Impiombato, A. Califano, A. Migliazza, G. Bhagat, R. Dalla-Favera, The DLEU2/miR-15a/16-1 cluster controls B cell proliferation and its deletion leads to chronic lymphocytic leukemia, Cancer Cell, 17 (2010) 28-40.

[9] V. Shukla, S. Ma, R.R. Hardy, S.S. Joshi, R. Lu, A role for IRF4 in the development of CLL, Blood, 122 (2013) 2848-2855.

[10] J. Durig, P. Ebeling, F. Grabellus, U.R. Sorg, M. Mollmann, P. Schutt, J. Gothert, L. Sellmann, S. Seeber, M. Flasshove, U. Duhrsen, T. Moritz, A novel nonobese diabetic/severe combined immunodeficient xenograft model for chronic lymphocytic leukemia reflects important clinical characteristics of the disease, Cancer Res, 67 (2007) 8653-8661.

[11] D. Bagnara, M.S. Kaufman, C. Calissano, S. Marsilio, P.E. Patten, R. Simone, P. Chum, X.J. Yan, S.L. Allen, J.E. Kolitz, S. Baskar, C. Rader, H. Mellstedt, H. Rabbani, A. Lee, P.K. Gregersen, K.R. Rai, N. Chiorazzi, A novel adoptive transfer model of chronic lymphocytic leukemia suggests a key role for T lymphocytes in the disease, Blood, 117 (2011) 5463-5472.

[12] S.E. Herman, X. Sun, E.M. McAuley, M.M. Hsieh, S. Pittaluga, M. Raffeld, D. Liu, K. Keyvanfar, C.M. Chapman, J. Chen, J.J. Buggy, G. Aue, J.F. Tisdale, P. Perez-Galan, A. Wiestner,

Modeling tumor-host interactions of chronic lymphocytic leukemia in xenografted mice to study tumor biology and evaluate targeted therapy, Leukemia, 27 (2013) 2311-2321.
[13] B.H. Mavromatis, B.D. Cheson, Pre- and post-treatment evaluation of non-Hodgkin's lymphoma, Best Pract Res Clin Haematol, 15 (2002) 429-447.
[14] B.D. Cheson, J.M. Bennett, M. Grever, N. Kay, M.J. Keating, S. O'Brien, K.R. Rai, National Cancer Institute-sponsored Working Group guidelines for chronic lymphocytic leukemia: revised guidelines for diagnosis and treatment, Blood, 87 (1996) 4990-4997.
[15] B.F. Eichhorst, K. Fischer, A.M. Fink, T. Elter, C.M. Wendtner, V. Goede, M. Bergmann, S. Stilgenbauer, G. Hopfinger, M. Ritgen, J. Bahlo, R. Busch, M. Hallek, C.L.L.S.G. German, Limited clinical relevance of imaging techniques in the follow-up of patients with advanced chronic lymphocytic leukemia: results of a meta-analysis, Blood, 117 (2011) 1817-1821.
[16] J.C. Byrd, J.M. Pagel, F.T. Awan, A. Forero, I.W. Flinn, D.P. Deauna-Limayo, S.E. Spurgeon, L.A. Andritsos, A.K. Gopal, J.P. Leonard, A.J. Eisenfeld, J.E. Bannink, S.C. Stromatt, R.R. Furman, A phase 1 study evaluating the safety and tolerability of otlertuzumab, an anti-CD37 mono-specific ADAPTIR therapeutic protein in chronic lymphocytic leukemia, Blood, 123 (2014) 1302-1308.
[17] M. Gentile, G. Cutrona, S. Molica, F. Ilariucci, F.R. Mauro, N. Di Renzo, F. Di Raimondo, I. Vincelli, K. Todoerti, S. Matis, C. Musolino, S. Fabris, M. Lionetti, L. Levato, S. Zupo, F. Angrilli, U. Consoli, G. Festini, G. Longo, A. Cortelezzi, P. Musto, M. Federico, A. Neri, M. Ferrarini, F. Morabito, Prospective validation of predictive value of abdominal computed tomography scan on time to first treatment in Rai 0 chronic lymphocytic leukemia patients: results of the multicenter O-CLL1-GISL study, Eur J Haematol, 96 (2016) 36-45.
[18] J.M. Froehlich, M. Triantafyllou, A. Fleischmann, P. Vermathen, G.N. Thalmann, H.C. Thoeny, Does quantification of USPIO uptake-related signal loss allow differentiation of benign and malignant normal-sized pelvic lymph nodes?, Contrast Media Mol Imaging, 7 (2012) 346-355.
[19] R. Weissleder, G. Elizondo, J. Wittenberg, C.A. Rabito, H.H. Bengele, L. Josephson, Ultrasmall superparamagnetic iron oxide: characterization of a new class of contrast agents for MR imaging, Radiology, 175 (1990) 489-493.
[20] R. Weissleder, P.F. Hahn, D.D. Stark, G. Elizondo, S. Saini, L.E. Todd, J. Wittenberg, J.T. Ferrucci, Superparamagnetic iron oxide: enhanced detection of focal splenic tumors with MR imaging, Radiology, 169 (1988) 399-403.
[21] Y.Z. Wadghiri, J. Li, J. Wang, D.M. Hoang, Y. Sun, H. Xu, W. Tsui, Y. Li, A. Boutajangout, A. Wang, M. de Leon, T. Wisniewski, Detection of amyloid plaques targeted by bifunctional

USPIO in Alzheimer's disease transgenic mice using magnetic resonance microimaging, PLoS One, 8 (2013) e57097.

[22] A. Crimi, O. Commowick, A. Maarouf, J.C. Ferre, E. Bannier, A. Tourbah, I. Berry, J.P. Ranjeva, G. Edan, C. Barillot, Predictive value of imaging markers at multiple sclerosis disease onset based on gadolinium- and USPIO-enhanced MRI and machine learning, PLoS One, 9 (2014) e93024.

[23] T. Tourdias, S. Roggerone, M. Filippi, M. Kanagaki, M. Rovaris, D.H. Miller, K.G. Petry, B. Brochet, J.P. Pruvo, E.W. Radue, V. Dousset, Assessment of disease activity in multiple sclerosis phenotypes with combined gadolinium- and superparamagnetic iron oxide-enhanced MR imaging, Radiology, 264 (2012) 225-233.

[24] M. Marinescu, F. Chauveau, A. Durand, A. Riou, T.H. Cho, A. Dencausse, S. Ballet, N. Nighoghossian, Y. Berthezene, M. Wiart, Monitoring therapeutic effects in experimental stroke by serial USPIO-enhanced MRI, Eur Radiol, 23 (2013) 37-47.

[25] Y.L. Wu, Q. Ye, K. Sato, L.M. Foley, T.K. Hitchens, C. Ho, Noninvasive evaluation of cardiac allograft rejection by cellular and functional cardiac magnetic resonance, JACC Cardiovasc Imaging, 2 (2009) 731-741.

[26] A.M. Lutz, C. Seemayer, C. Corot, R.E. Gay, K. Goepfert, B.A. Michel, B. Marincek, S. Gay, D. Weishaupt, Detection of synovial macrophages in an experimental rabbit model of antigen-induced arthritis: ultrasmall superparamagnetic iron oxide-enhanced MR imaging, Radiology, 233 (2004) 149-157.

[27] K. Tsuchiya, N. Nitta, A. Sonoda, H. Otani, M. Takahashi, K. Murata, M. Shiomi, Y. Tabata, S. Nohara, Atherosclerotic imaging using 4 types of superparamagnetic iron oxides: new possibilities for mannan-coated particles, Eur J Radiol, 82 (2013) 1919-1925.

[28] C. Bremer, T. Allkemper, J. Baermig, P. Reimer, RES-specific imaging of the liver and spleen with iron oxide particles designed for blood pool MR-angiography, J Magn Reson Imaging, 10 (1999) 461-467.

[29] S. Metz, G. Bonaterra, M. Rudelius, M. Settles, E.J. Rummeny, H.E. Daldrup-Link, Capacity of human monocytes to phagocytose approved iron oxide MR contrast agents in vitro, Eur Radiol, 14 (2004) 1851-1858.

[30] J. Gellissen, C. Axmann, A. Prescher, K. Bohndorf, K.P. Lodemann, Extra- and intracellular accumulation of ultrasmall superparamagnetic iron oxides (USPIO) in experimentally induced abscesses of the peripheral soft tissues and their effects on magnetic resonance imaging, Magn Reson Imaging, 17 (1999) 557-567.

[31] F. Morabito, G. Cutrona, M. Gentile, S. Fabris, S. Matis, E. Vigna, K. Todoerti, M. Colombo, A.G. Recchia, S. Bossio, L. De Stefano, F. Ilariucci, A. Cortelezzi, U. Consoli, I. Vincelli, E.A. Pesce, C. Musolino, S. Molica, F. Di Raimondo, A. Neri, M. Ferrarini, Is ZAP70 still a key prognostic factor in early stage chronic lymphocytic leukaemia? Results of the analysis from a prospective multicentre observational study, Br J Haematol, 168 (2015) 455-459.
[32] F. Morabito, L. Mosca, G. Cutrona, L. Agnelli, G. Tuana, M. Ferracin, B. Zagatti, M. Lionetti, S. Fabris, F. Maura, S. Matis, M. Gentile, E. Vigna, M. Colombo, C. Massucco, A.G. Recchia, S. Bossio, L. De Stefano, F. Ilariucci, C. Musolino, S. Molica, F. Di Raimondo, A. Cortelezzi, P. Tassone, M. Negrini, S. Monti, D. Rossi, G. Gaidano, M. Ferrarini, A. Neri, Clinical monoclonal B lymphocytosis versus Rai 0 chronic lymphocytic leukemia: A comparison of cellular, cytogenetic, molecular, and clinical features, Clin Cancer Res, 19 (2013) 5890-5900.
[33] P. Foster-Gareau, C. Heyn, A. Alejski, B.K. Rutt, Imaging single mammalian cells with a 1.5 T clinical MRI scanner, Magn Reson Med, 49 (2003) 968-971.
[34] S.D. Wolff, R.S. Balaban, Assessing contrast on MR images, Radiology, 202 (1997) 25-29.
[35] H.E. Daldrup-Link, M. Rudelius, G. Piontek, S. Metz, R. Brauer, G. Debus, C. Corot, J. Schlegel, T.M. Link, C. Peschel, E.J. Rummeny, R.A. Oostendorp, Migration of iron oxide-labeled human hematopoietic progenitor cells in a mouse model: in vivo monitoring with 1.5-T MR imaging equipment, Radiology, 234 (2005) 197-205.
[36] K.K. Wong, F. Brenneman, A. Chesney, D.E. Spaner, R.M. Gorczynski, Soluble CD200 is critical to engraft chronic lymphocytic leukemia cells in immunocompromised mice, Cancer Res, 72 (2012) 4931-4943.
[37] G. Baio, M. Fabbi, D. de Totero, S. Ferrini, M. Cilli, L.E. Derchi, C.E. Neumaier, Magnetic resonance imaging at 1.5 T with immunospecific contrast agent in vitro and in vivo in a xenotransplant model, MAGMA, 19 (2006) 313-320.
[38] G.H. Simon, J. Bauer, O. Saborovski, Y. Fu, C. Corot, M.F. Wendland, H.E. Daldrup-Link, T1 and T2 relaxivity of intracellular and extracellular USPIO at 1.5T and 3T clinical MR scanning, Eur Radiol, 16 (2006) 738-745.
[39] P.E. Patten, G. Ferrer, S.S. Chen, R. Simone, S. Marsilio, X.J. Yan, Z. Gitto, C. Yuan, J.E. Kolitz, J. Barrientos, S.L. Allen, K.R. Rai, T. MacCarthy, C.C. Chu, N. Chiorazzi, Chronic lymphocytic leukemia cells diversify and differentiate in vivo via a nonclassical Th1-dependent, Bcl-6-deficient process, JCI Insight, 1 (2016).

Figures captions

Fig. 1. Representative slices of the sequence protocol used to measure the signal intensity (SI) in tissues of interest

The regions of interest (ROIs, white circles) were drawn in the tissues of interest, spleen and in the region outside the anatomy of the mice (background noise) in order to measure the signal intensity (SI), as mean ± standard deviation (SD) and to calculate the signal-to-noise ratio (SNR) as described in Materials and Methods section.

Fig. 2. Magnetic resonance image signal determination and histological analysis in control (NSG-CTR) compared to engrafted (NSG-CLL) mice

The figure shows representative *in vivo* USPIO magnetic resonance images (MRI) obtained after 24 h of USPIO administration in a NSG-CTR (A) and NSG-CLL mouse (D). The position of the spleen is indicated by the red outline. Matched histology sections (magnification, 100X) show the absence (B) or the presence (E) of CD20 (red) and Ki67 (brown) positive cells; Perls' Prussian blue ferric iron staining (C and F) allows the detection of USPIO nanoparticles.

Fig. 3. Comparison of magnetic resonance image signal intensity change in the spleen of control (NSG-CTR), engrafted (NSG-CLL) at 2 and 4 weeks and non-engrafted (NSG-ne) mice.

(A) The scatter dot plot represents percentage Signal-to-Noise ratio change (ΔSNR%) of the MRI acquisition analysis comparing NSG-CLL mice at 2 weeks (red dots) and 4 weeks (blue dots) from peripheral blood mononuclear cell (PBMC) CLL injection, NSG-CTR mice (black dots) and NSG-ne (grey dots, evaluated at 4 weeks from PBMC CLL injection). Values of ΔSNR% are expressed as mean±sem. NSG-CTR mice: -42.16±5.6; NSG-CLL at 2 weeks: +16.32±3.95; NSG-CLL at 4 weeks: +30.49±4.0; NSG-CLL-ne mice: -37.21±5.5. Statistical comparisons were carried out using the U-Mann-Whitney test. A P-value<0.0001 is indicated by *** and P=0.017 by *. (B) Comparison of MRI signals detected in the same mice 2 weeks (red dots) or 4 weeks (blue dots) from PBMC CLL injection (P=0.02 Wilcoxon-matched pair test).

Fig. 4 Representative experiment of treatment with rituximab

The figure shows a representative *in vivo* USPIO magnetic resonance image (MRI) obtained 24 h after USPIO administration in a NSG-CLL mouse treated with saline solution (A) and a NSG-CLL mouse treated with rituximab (B). The position of the spleen is indicated by the red outline. MRI images show acquisition at therapy start (T.S.) and at therapy completion (T.C). The scatter dot plots (C) and (D) display data for each mouse and percentage Signal-to-Noise ratio change (ΔSNR%) mean values are calculated for each treatment-mice group (n=3) and the control NSG-CTR group.

Fig. 5. Representative immunohistochemistry and flow cytometry analysis of mouse spleens from a rituximab experiment

The figure shows the histologic analysis carried out for the presence of CLL cells (CD20, red), proliferating cells (Ki67, brown), T cells (CD3, red) and USPIO nanoparticles (Perls' Prussian blue) in the NSG-CLL mice treated with saline solution (A) and in NSG-CLL mice treated with rituximab (B). Magnification 40X (left panels) and 200X (right panels).

In panels C and D, the scatter-plots show the presence of CLL cells and autologous T-cells, respectively, evaluated by flow cytometry (CD45+/CD19+/CD5+ or CD45+/CD19-/CD5+), indicating a significant decrease of the percentage of CLL cells in the group of mice treated with rituximab (n=4) compared to the control group treated with saline solution (n=5). Statistical comparisons were carried out by Wilcoxon test.

Table 1. Biologic and molecular characteristics of CLL patients included in the study.

Prognostic parameters	**n (% of total)**
CD38	
Negative	13 (72.2)
Positive	5 (27.8)
Total	18 (100)
ZAP-70	
Negative	6 (33.3)
Positive	12 (66.7)
Total	18 (100)
IGHV	
Mutated	13 (72.2)
Unmutated	5 (27.8)
Total	18 (100)
FISH	
Negative	3 (17.6)
del(13)(q14)	14 (82.4)
trisomy 12	0 (0)
del(11)(q22.3)	0 (0)
del(17)(p13)	0 (0)
Total	17 (100)

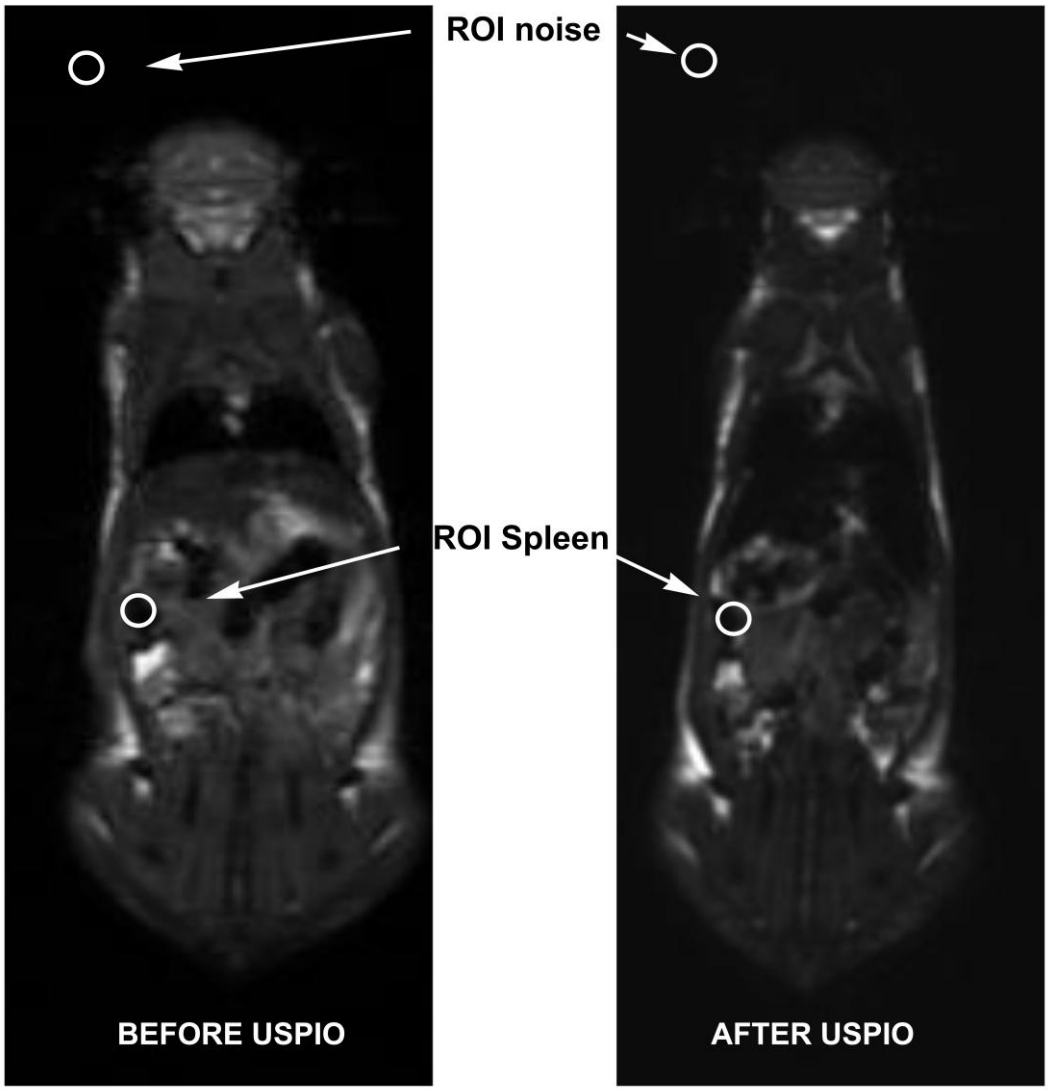

Fig. 1

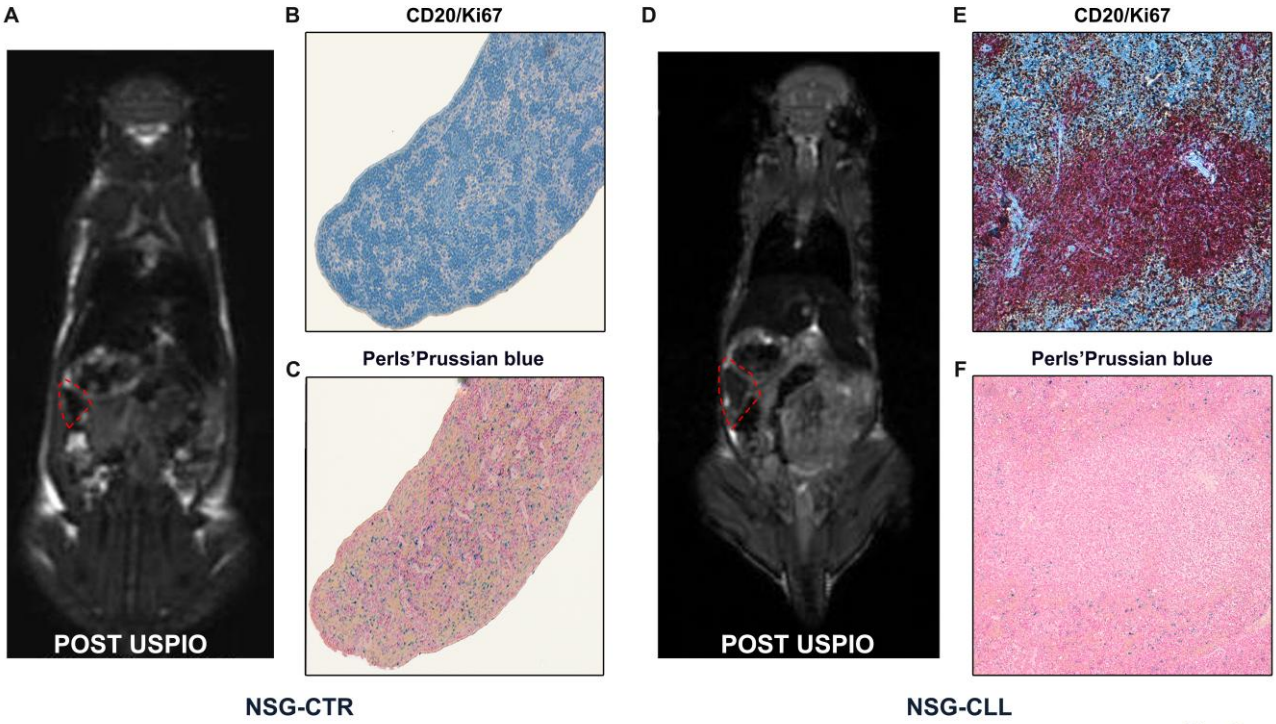

Fig. 2

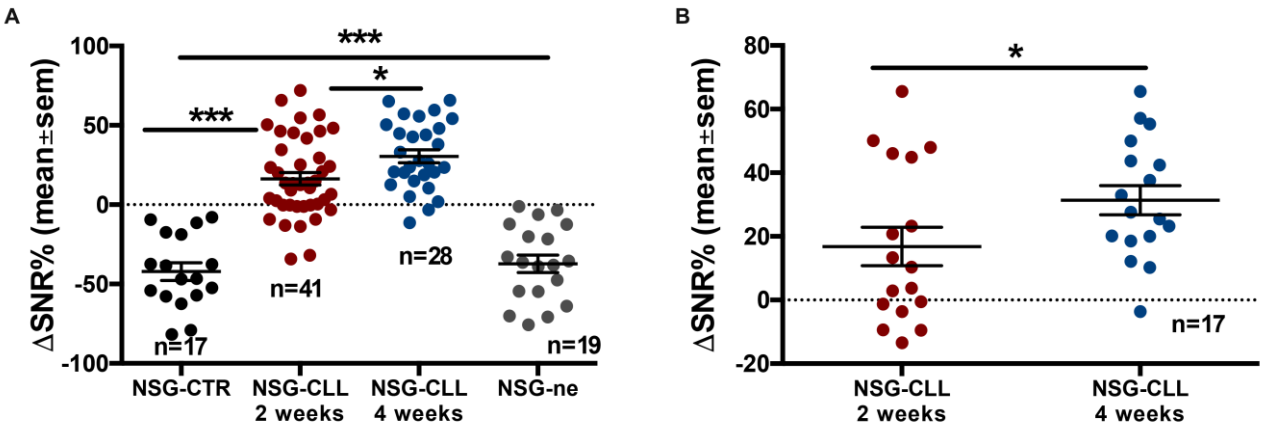

Fig. 3

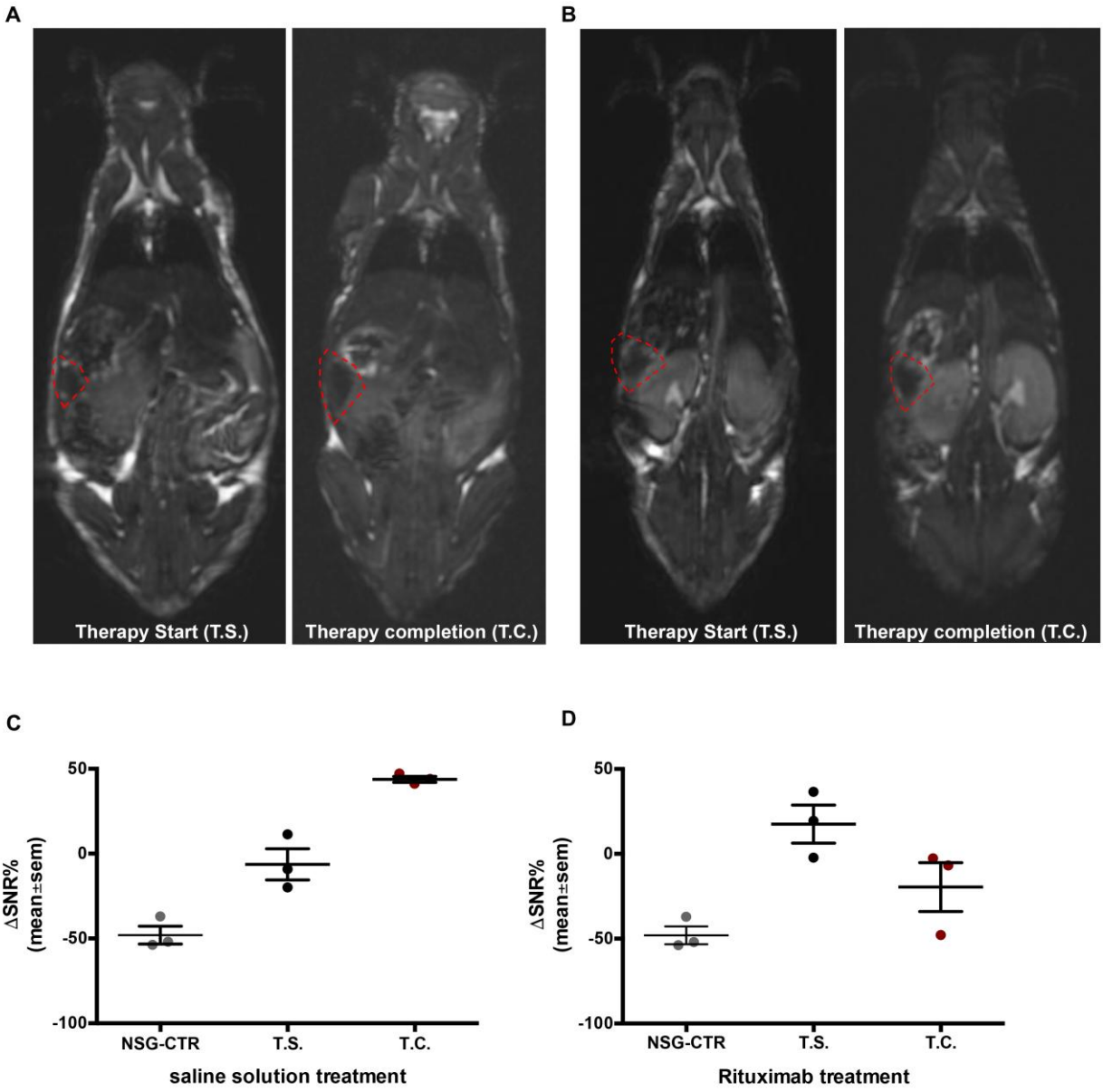

Fig. 4

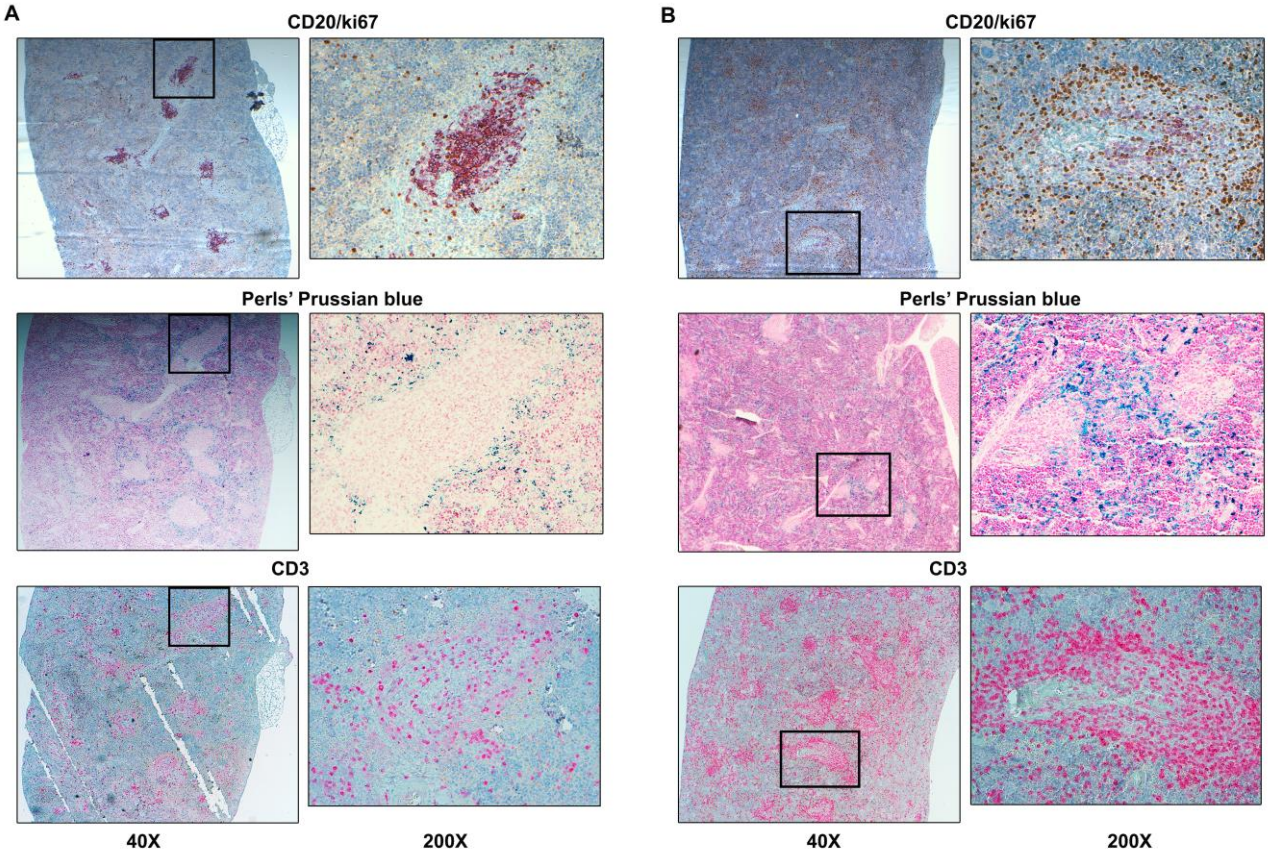

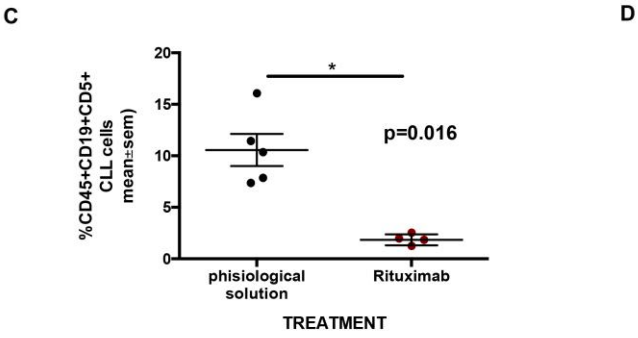

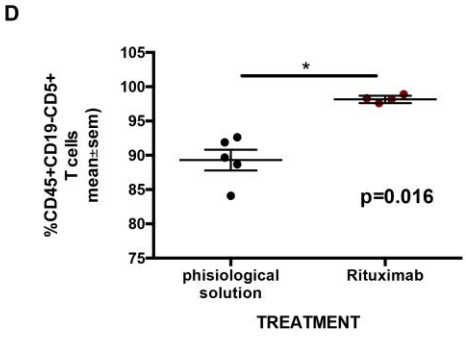

Fig. 5

Highlights

- Non-invasive specific MRI method to monitor the CLL disease progression in a xenograft mouse model
- reduction of the mice number to be used and sacrificed in each experimental sett
- Early and precise detection of the CLL cell graft take in NGS mice: cell engrafment is already evident two weeks following injection potential applications for staging and therapy monitoring in humans.